Research Article

Effect of gadolinium doped ZnS nanoparticles: ferro magnetic photocatalyst for efficient dye degradation

R. Sanjeev Kumar[1,2] · V. Veeravazhuthi[2] · N. Muthukumarasamy[1] · M. Thambidurai[3] · M. Elango[2] · A. Gnanaprakasam[4] · G. Rajesh[1,5]

Abstract
In the present work, solution based simple chemical precipitation method has been used to prepare undoped and Gd doped ZnS nanoparticles. The prepared nanoparticles were characterized by standard analytical methods the X-ray diffraction results revealed that the undoped and Gd doped ZnS nanoparticles corresponds to hexagonal wurtizite structure. The FESEM images shows that the formation of agglomerated nanoparticles. The compositional analysis confirmed the presence of Gd in ZnS matrix with reasonable dissolution range. HRTEM results show that undoped and Gd doped ZnS nanoparticles exhibit a uniform size distribution with average grain size lying in the range of 2.4–3.9 nm. The magnetic studies of Gd doped ZnS nanoparticles carried out at room temperature by vibrating sample magnetometer shows that the materials exhibit magnetic hysteresis. The prepared samples shows paramagnetic behavior at room temperature. The degradation of methylene blue dye (MB), methyl orange dye (MO) and effluent collected from industry by the undoped and Gd doped ZnS nanoparticles was studied using 8 W, UV visible lamp light irradiation. The color degradation efficiency for MB is found to be 95%, whereas the color degradation efficiency for MO is 97% and for the effluent collected from a dye industry it was nearly 90%.

Keywords Chemical precipitation method · Gd doped ZnS · XRD · HRTEM

1 Introduction

Waste water from industries, factories, laboratories etc. causes serious problems to the environment. The release of waste containing dyes is toxic to microorganisms, aquatic life and human beings [1]. The chemicals such as azo dyes, herbicides, and pesticides are present in rivers and lakes, and are in part suspected of being endocrine-disrupting chemicals (EDCs) [2–4]. Environmental problems related with hazardous wastes and toxic water-pollutants have attracted much attention in recent years. Organic dyes are one of the major group of pollutants in waste water released from textile and other industrial processes. Especially, Textile dyes and other industrial dyestuffs constitute one of the largest groups of organic compounds that represent an increasing environmental danger [5]. Among the various physical and biological techniques available for the treatment of pollutants, the methods like precipitation, adsorption, air stripping, flocculation, reverse osmosis, and ultra-filtration can be used for color removal of textile effluents [6–8]. Advanced oxidation processes are an alternative methodology for the annihilation of many organics elements in wastewater. Zn based semiconductor mediated photocatalysis is a well established photocatalyst, which can be expediently used for the total destruction of toxic organic compounds into

✉ R. Sanjeev Kumar, sanjeev.phy@gmail.com | [1]Department of Physics, Coimbatore Institute of Technology, Coimbatore, Tamil Nadu, India. [2]Department of Physics, PSG College of Arts and Science, Coimbatore, Tamil Nadu, India. [3]Department of Electrical and Electronic Engineering, Nanyang Technological University, Singapore, Singapore. [4]Department of Chemical Engineering, Coimbatore Institute of Technology, Coimbatore, Tamil Nadu, India. [5]Millennium Nucleus Multimat, Santiago, Chile.

SN Applied Sciences (2019) 1:268 | https://doi.org/10.1007/s42452-019-0283-0

Received: 26 September 2018 / Accepted: 18 February 2019 / Published online: 26 February 2019

non-toxic compounds [9–13]. ZnS is one of the important II–VI semiconductor material with wide band gap energy of 3.5–3.7 eV for cubic zinc blend structure and 3.7–3.8 eV for hexagonal wurtzite structure [14]. Recently, transition-metal sulfides, in particular ZnS, has attracted much interest because of its potential applications in the field of electronic devices and catalysis [15]. In the last few years, semiconductor materials as heterogeneous photocatalysts have been used in wastewater treatments [16, 17]. Because of the low cost, high efficiency, commercial availability and high chemical stability, the semiconductor based photocatalytic method is being considered as the best alternative method for the treatment of wastewater. Photocatalysts with high porosity provides uniform and amendable environment for the destruction of toxic organic pollutants that enhances the photocatalytic degradation efficiency. Recently, ZnS is used as most efficient photocatalyst for the treatment of toxic organic effluents [18–21]. Zinc sulfide absorbs the light under UV region, but its absorbance capacity can be further tuned by adding various transition metal ions as dopant. Acting as an electron and/or hole trap is the most important function of these dopants. The trapping of charge carriers decreases the recombination rate of electron–hole pairs and consequently, increases the life time of charge carriers resulting in an enhancement in photocatalytic activity [22].

In this work, undoped and Gd doped ZnS nanoparticles have been prepared via chemical precipitation method. The prepared materials were characterized by XRD, FE-SEM, EDX, HR-TEM, UV–Vis, and VSM to study the structural, optical and magnetic properties of prepared samples. Photodegradation of methylene blue dye (MB), methyl orange dye (MO) and effluent from industry was studied to check the photocatalytic activity of pure and Gd Doped ZnS under UV irradiation.

2 Experimental

2.1 Synthesis of undoped and Gd doped ZnS nanoparticles

Synthesis of undoped and Gd doped ZnS nanoparticles was carried out by simple chemical precipitation method. Aqueous solution of zinc acetate [$(CH_3COO)_2$ Zn·$2H_2O$] and required amount of gadolinium nitrate [(Gd $(NO_3)_2$·H_2O] were stirred separately for an hour at room temperature. Solution A was prepared by mixing the zinc and gadolinium precursor solution and solution B was prepared by dissolving sodium sulfide (Na_2S) in 100 ml of aqueous medium and is stirred for 2 h, due to the addition of sodium sulfide solution in solution A, the color of the medium changes to ivory precipitate which is the indication of formation of gadolinium doped ZnS nanoparticles. In order to remove the unreacted precursor and surface adhered organic impurities, the above prepared precipitate was washed with double distilled water and rinsed with organic solvents such as acetone and ethanol. Finally, the precipitate was centrifuged at 2500 rpm for 10 min and dried in hot air oven for 6 h at 100 °C. The dried nanoparticles were annealed at 300 °C for 2 h. Finally, the dried powder was crushed in the agate mortar to obtain Gd doped ZnS nanoparticles 2.17% and 3.93% Gd doped ZnS nanoparticles have been prepared.

2.2 Characterization

The structural properties of the prepared nanoparticles were studied using X-ray diffraction method using PANalytical X-ray diffractometer, the surface morphology of the samples has been studied using JEOL JEM-6390 scanning electron microscope (SEM), the composition of the prepared samples has been studied using energy dispersive X-ray analysis (EDAX, Thermo-Noran system Six) and the high resolution transmission electron microscope (HRTEM) images of the prepared ZnS and Gd doped ZnS samples have been recorded using a JEOL JEM 2100 microscope. The optical properties have been studied using the absorbance spectrum recorded using spectrophotometer (JASCO-V-570). The magnetization measurements of prepared undoped and Gd-doped ZnS samples were recorded using a vibrating sample magnetometer (Make: Lake Shore, Model: 7404).

2.3 Photocatalytic activity on industrial effluent

The degradation of methylene blue dye (MB), methyl orange dye (MO) and effluent from industry by the undoped and Gd doped ZnS nanoparticles was studied using 8 W, UV visible lamp with wavelength 365 nm. Different concentrations of dye solutions were prepared. 30 ml of dye solution was taken from the prepared stock solution (50 ppm) and was dissolved in 70 ml of double distilled water to get a concentration of 15 ppm. 100 mg of photocatalyst (undoped and Gd doped ZnS nanoparticles) was used for photocatalytic degradation study. The evaluation was carried out on all samples for 300 min of irradiation time. The percentage of degradation of color was determined using the equation [23].

$$D\% = 100 \times \frac{C_0 - C_t}{C_0} = 100 \times \frac{A_0 - A_t}{A_0}$$

where C_o and C_t are the initial concentration and concentration of dye at time t. A_o and A_t are initial and final absorbance at time t. D is the degradation efficiency.

3 Result and discussion

$$(d_{hkl})^{-2} = \frac{4}{3}\frac{h^2 + hk + k^2}{a^2} + \left(\frac{l}{c}\right)^2$$

Figure 1 shows the XRD patterns of the prepared ZnS and Gd doped ZnS samples. All the samples show three diffraction peaks. All the peaks in the diffraction pattern are found to be characteristic of the hexagonal phase of ZnS. The observed diffraction peaks at 2θ (°) values of 27.92°, 47.62° and 56.11° have been assigned to the (101), (110) and (114) planes of hexagonal ZnS. The observed diffraction peaks are in good agreement with JCPDS data (indexed with JCPDS Card No. 89-7385). No additional peaks are obtained in case of doped samples but there is a slight shift in 2θ values. This observation reveals that the hexagonal structure of the ZnS is unaltered and further indicates that the dopant Gd replaces some of the Zn in the parent (ZnS) material. The lattice constants a and c have been determined from the interplanar spacing of the different (hkl) planes using the relation.

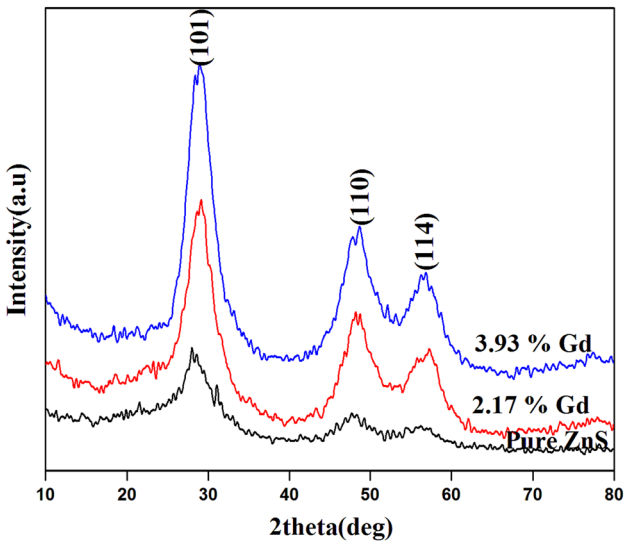

Fig. 1 X-ray diffraction pattern of undoped and Gd doped ZnS nanoparticles

It is observed that the lattice constants 'a' and 'c' decreases with increase in Gd concentration. Table 1 shows the structural parameters of the Gd doped ZnS nanoparticles. It is also seen that the Bragg angle (2θ) of the intense (101) reflection exhibits a slight shift towards higher 2θ values with increase in Gd concentration. The absence of the diffraction peaks of GdS phase in the pattern implies that Gd substitutes for Zn in the prepared Gd doped ZnS. No other impurity phase is observed, which indicates that the Gd ion occupies the lattice site rather than the interstitial ones. The grain size values of the particles have been calculated using Scherrer's formula

$$D = \frac{K\lambda}{\beta \cos\theta}$$

where D is the grain size, K is a constant taken to be 0.94, λ is the wavelength of the X-ray radiation, β is the full width at half maximum and θ is the angle of diffraction. The average grain size of undoped ZnS is found to be 2.6 nm. The average grain size of has been calculated and is found to be 3.8 nm for 2.17% Gd doped ZnS and 4.6 nm for 3.93% Gd doped ZnS respectively. Similar result has been reported by Divya et al. [24]. The calculated values of lattice parameters are found to decrease with increasing Gd.

The surface morphology of undoped and Gd doped ZnS samples has been studied using FESEM. Figure 2a–c shows the FESEM images of the prepared ZnS and Gd doped (2.17% and 3.93%) nanocrystalline ZnS samples. The FESEM images show that the particles have smooth surface and the material contains agglomerated nanoparticles and there is uniform distribution of particles. The elemental composition of the synthesized ZnS and Gd doped ZnS have been determined through the energy dispersive X-ray analysis (EDAX). Figure 3a–c shows the energy dispersive X-ray analysis of the undoped and Gd doped ZnS. EDAX analysis reveals the presence of Zn, Gd and S in the samples and the amount of Zn is found to decrease with the increase of Gd concentration.

Figure 4 shows the HRTEM images of undoped and Gd doped ZnS nanoparticles. Figure 4b, d, f shows the lattice fringes and the lattice spacing values have been determined using these fringes. The d-spacing was found to be 3.206 A°, 3.114 A°, 3.093 A° for undoped, 2.17% Gd and 3.93% Gd doped ZnS nanoparticles respectively. The

Table 1 Structural parameters of undoped and Gd-doped ZnS

Sample	2θ (°) for most intense peak (101)	d spacing (Å)	Lattice parameter values		Grain size (nm)
			a (Å)	*c* (Å)	
ZnS	28.01	3.206	3.81	12.43	2.6
2.17 wt% Gd	28.80	3.114	3.79	12.37	3.8
3.93 wt% Gd	29.22	3.093	3.75	12.35	4.6

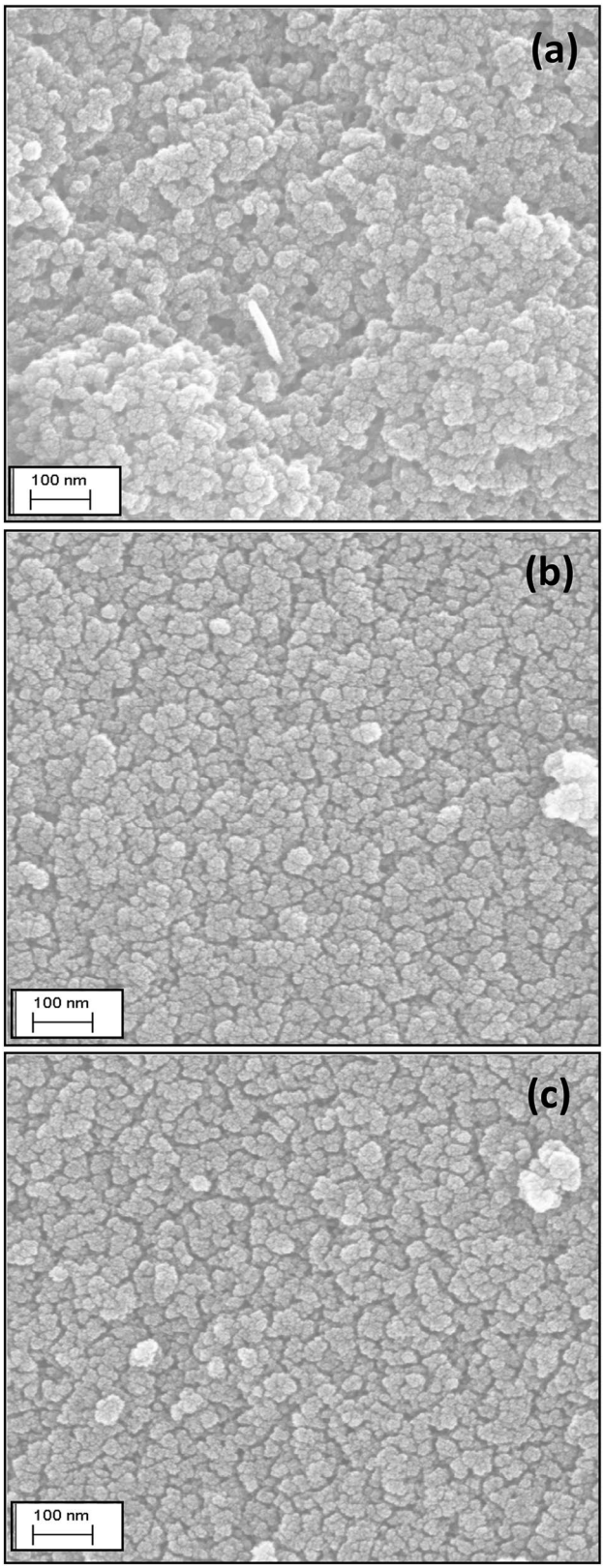

Fig. 2 FESEM images of **a** undoped ZnS, **b** 2.17% Gd doped ZnS and **c** 3.93% Gd doped ZnS nanoparticles

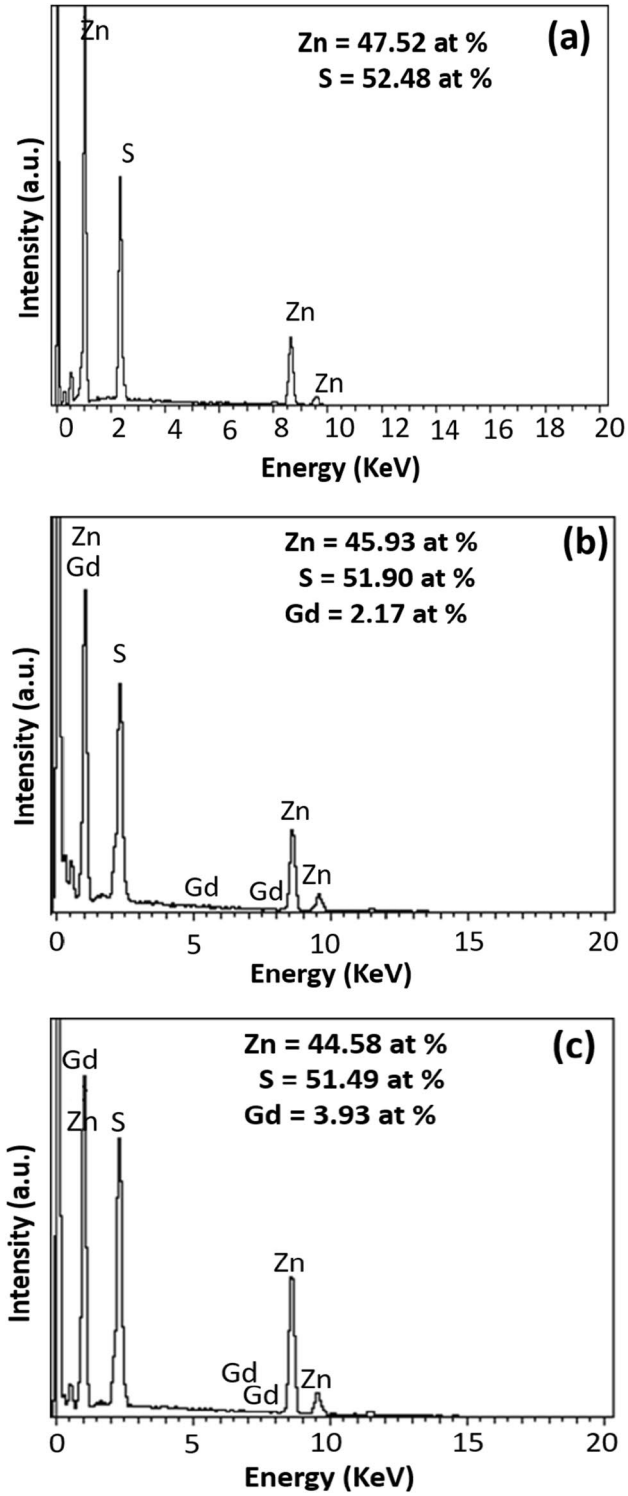

Fig. 3 EDAX pattern of **a** undoped ZnS, **b** 2.17% Gd doped ZnS and **c** 3.93% Gd doped ZnS nanoparticles

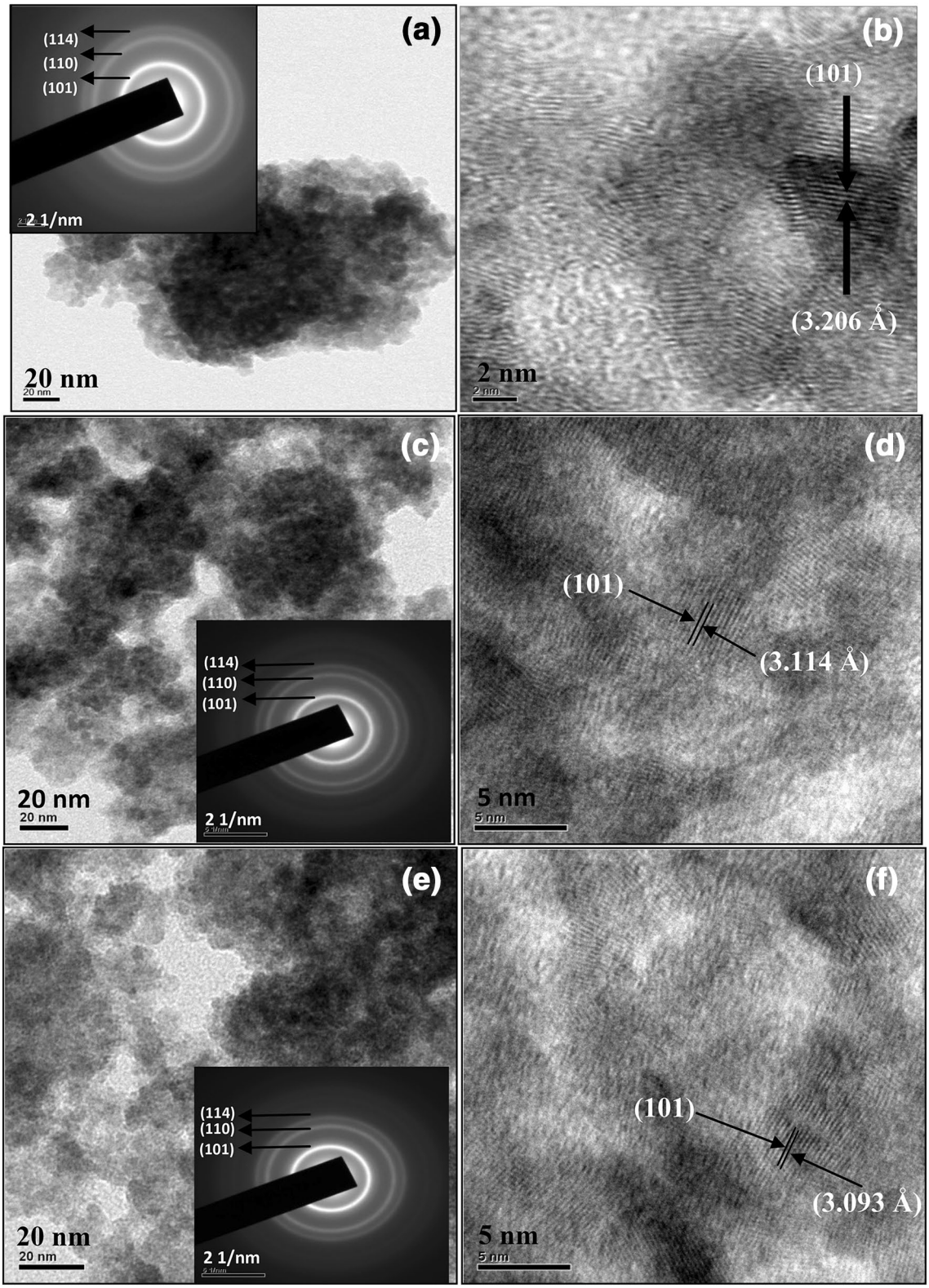

Fig. 4 HRTEM images **a**, **b** undoped ZnS, **c**, **d** 2.17% Gd doped ZnS and **e**, **f** 3.93% Gd doped ZnS nanoparticles

d-spacing values are observed to decrease due to small ionic radius of Gd when compared to that of Zn and S. The calculated values are in close agreement with the X-ray diffraction results. The crystallite size was found to lie in the range of 2.4–3.9 nm. Inset of Fig. 4a, c, e shows the selected area electron diffraction pattern of undoped ZnS, 2.17% Gd and 3.93% Gd doped ZnS nanoparticles respectively. The ring pattern shows that the synthesized samples are of nanocrystalline nature and also the prepared samples exhibit hexagonal wurtzite phase.

The UV–Vis optical absorption spectra of Gd doped ZnS nanoparticles were recorded in the range 250–550 nm and are shown in the Fig. 5. The band edge absorption occurs at 294 nm, 297 nm and 307 nm for undoped, 2.17% Gd and 3.93% Gd doped nanoparticles respectively. From the result it is clear that the prepared samples are in nano dimensional state, which obeys quantum confinement effect. For all the prepared samples, the absorption edge is shifted towards lower wavelength when compared to bulk ZnS systems (345 nm). It is observed that when the undoped ZnS is doped with different concentrations of Gd ions, the absorption edge is moved to higher wavelength region. The fundamental absorption which corresponds to electron excitation from the valance band to conduction band can be used to determine the value of the optical band gap of semiconductor system.

Further the band gap value was calculated using the relation between absorption coefficient (α) and incident photon (hu) which can be represented as,

$$(\alpha h\vartheta)^{1/n} = A\left(h\vartheta - E_g\right)$$

where α is absorption coefficient, A is constant, h is Planck constant and E_g is the optical band gap n = 1/2 for direct band gap material. The extrapolation of linear region of the plot $(\alpha hv)^2$ versus (hu) gives the band gap of the nanoparticles.

Tauc plots of undoped and Gd doped ZnS nanoparticles are shown in the Fig. 6. From the plots, we estimated the energy gap values of undoped, 2.17% and 3.93% Gd doped ZnS nanoparticles as 3.84 eV, 3.79 eV and 3.73 eV respectively. It is observed that the band gap shows a slight decrease with increasing Gd concentration.

Figure 7 shows the hysteresis loops of the Gd doped ZnS samples recorded at room temperature by vibrating sample magnetometer. The samples show paramagnetic in nature for undoped ZnS and ferromagnetic behavior for Gd doped ZnS nanoparticles at room temperature.

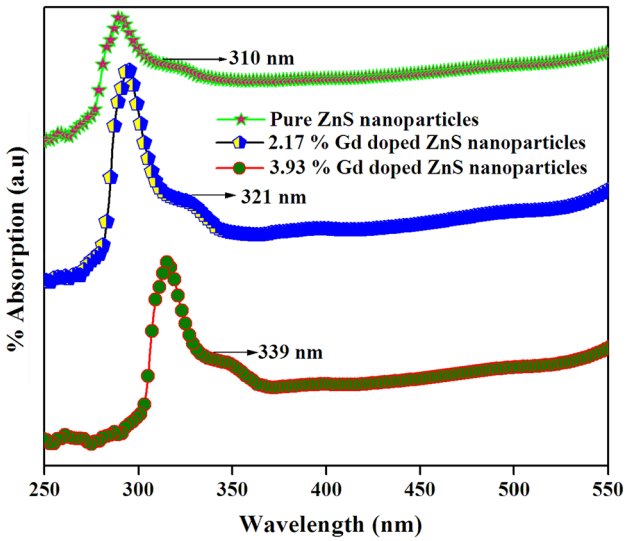

Fig. 5 Optical absorption spectra of undoped ZnS and Gd doped ZnS nanoparticles

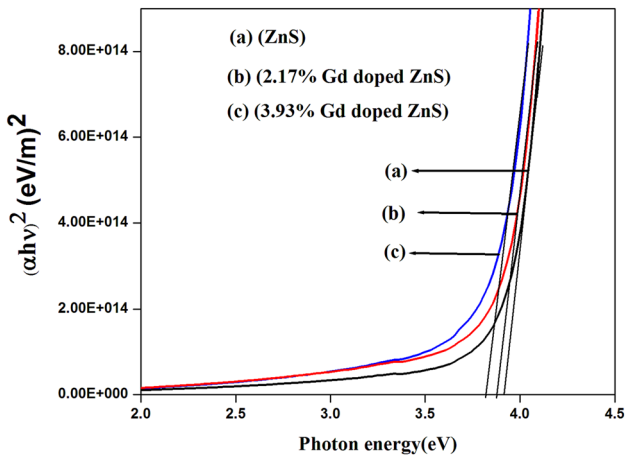

Fig. 6 Plot $(\alpha hv)^2$ versus photon energy (hv) of undoped ZnS and Gd doped ZnS nanoparticles

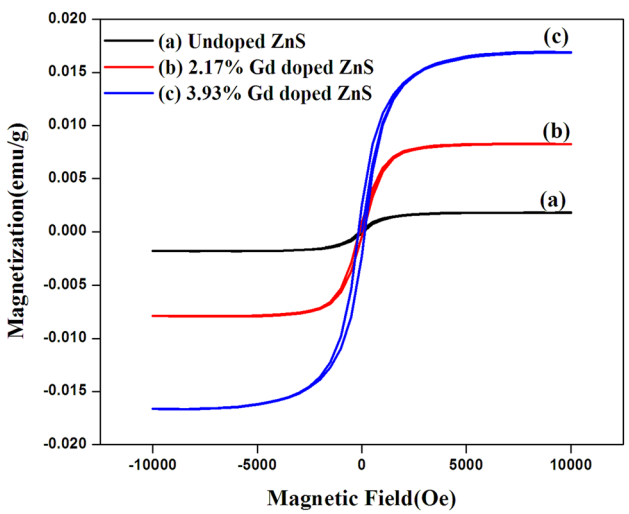

Fig. 7 M-H curve of undoped ZnS and Gd doped ZnS nanoparticles

This feature suggests that the introduction of Gd into ZnS causes effective coupling of magnetic ions within the sample. The saturation magnetization (M_s), remanent magnetization (M_r) and coercivity values of undoped and Gd doped ZnS samples are shown in Table 2. The, saturation magnetization has been found to increase with increase in doping concentration of 4*f* orbital dopants. Divya et al. [24] have reported that increase in saturation magnetization can be attributed to sulfur vacancies, which generate long range ferromagnetism. As the doping concentration of Gd ions increase there is an increase in sulfur vacancies and also a decrease in particle size. The saturation magnetization increases which is due to FM coupling among Gd ions. With increase in doping concentration, the curve, between magnetization and applied magnetic field, exhibit a linear trend, which can be expected to be presence of ferromagnetic behavior. The strong *sp-f* exchange interactions between ZnS and Gd ions are responsible for the induced magnetism. Thus, it is concluded that the cause of this magnetism is intrinsic, which arises due to the substitution of Zn by Gd ions. The observed room-temperature ferromagnetism may be due to the substitution of Gd^{3+} in place of Zn^{2+} in the zinc sulfide lattice without changing their structure. As the results of XRD did not expose the presence of any Gd impurity phases. Increase in the concentration of Gd-doping will decrease the distance among the Gd ions and enhance the magnetization [25].

Table 2 The magnetic parameters of undoped and Gd doped ZnS samples

Samples	Magnetization M_s (emu/g) (10^{-3})	Coericivity (H_{ci}) (Oe)	Retentivity M_r (emu/g) (10^{-6})
Undoped ZnS	1.7939	89.852	160.08
2.17 wt% Gd doped ZnS	8.1217	150.74	663.29
3.93 wt% Gd doped ZnS	16.800	134.41	678.21

In Gd doped ZnS dilute magnetic semiconductors, Rare earth (RE) metal ions exhibit larger magnetic moments due to their strong Ferro Magnetic (FM) coupling between *f*-electron of RE ions and *s*-electrons of the host semiconductor. However, still it is not convincing, due to the controversial reports on the origin of ferromagnetism in RE-doped semiconductors. ZnS with 2.17% and 3.93% Gd exhibits room temperature ferromagnetism which corresponds to the FM coupling between *s*-electrons of the ZnS and *f*-electron of Gd ion. On further increasing the Gd concentration the paramagnetic contribution is enhanced due to large number of localized 4*f* electrons in Gd ions. Unlike 3*d* transition metal ions 4*f* RE electrons are localized, therefore the ferromagnetic coupling occurs indirectly via 5*d* or 6*s* conduction electrons. Further, special features of Gd such as having the partially filled 4*f* and 5*d* orbitals may lead to new exchange mechanisms through intra-ion and inter ion coupling and induce ferromagnetism [26].

In general, the photocatalytic degradation process consists of the following steps (1) adsorption–desorption of species, (2) generation of electron–hole pairs, (3) recombination of electron–hole pair and (4) surface reaction. The general mechanism of photocatalytic degradation of organic molecules is depicted in schematic diagram Fig. 8.

In general, the kinetics of photocatalytic degradation of organic molecule could be written in the form of Eq. (1).

$$\frac{dC_A}{dt} = kC_A^n \quad (1)$$

where k is the degradation rate constant, C_A is the concentration of dye solution, n is the order and t is the time

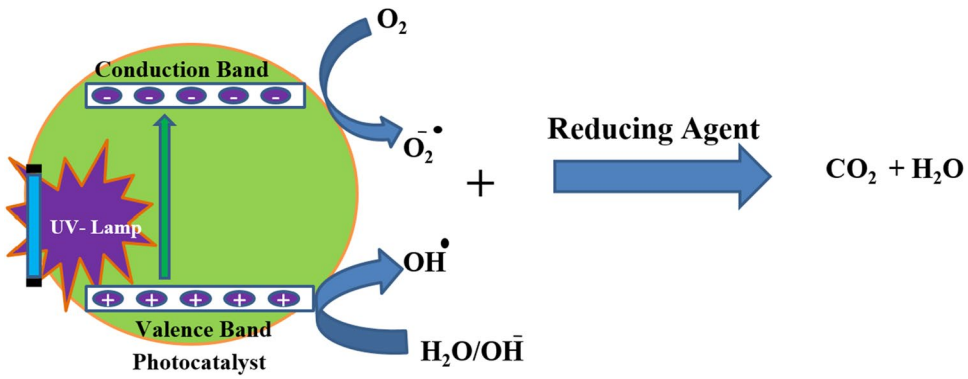

Fig. 8 Schematic diagram of photocatalytic degradation of organic effluent

for degradation. Assuming pseudo first order kinetics (i.e. n = 1) and integrating the above equation from t = 0, $C_A = C_{A0}$ to time t = t, $C_A = C_A$, the resulting equation can be re-written in the form of Eq. (2)

$$\ln\left(C_{Ao}/C_A\right) = kt \quad (2)$$

Figure 9a, b compares decolorization performance of prepared nanomaterials. The calculated decolonization percentage of ZnS nanoparticles is 95.45% with rate constant of 0.0111 min^{-1}. Meanwhile, Gd doped ZnS nanoparticles exhibited 97.34% degradation percentage for both 2.17% Gd and 3.93% in 5 h duration reaction with rate constants of 0.0117 min^{-1} respectively (Table 3). Figure 9c shows the UV–Vis absorption spectra for 3.93% Gd doped ZnS NPs at different period of time intervals and it could be notice there is no peaks observed other than methylene blue (MB) dye solution which confirms that complete degradation methylene blue MB dye solution.

For methyl orange (MO) a colour removal efficiency of 99.70% was obtained with rate constant of 0.0128 min^{-1}. For Gd doped ZnS nanoparticles, the photocatalytic degradation percentage are found to be 97.50% for 2.17% Gd and 89.70% for 3.93% Gd doped ZnS. The calculated rate constant (k) for 2.17% Gd and 3.93% Gd doped ZnS were 0.0122 min^{-1} and 0.0100 min^{-1} respectively (Fig. 10a, b). From the Fig. 10c, complete degradation of methyl orange (MO) confirmed.

Photo catalytic degradation of the industrial effluent was studied and it was observed that the colour degradation efficiency is 89.47% for undoped ZnS with rate constant of 0.0063 min^{-1} (Fig. 11a, b). For Gd doped ZnS nanoparticles, the photocatalytic colour degradation percentage were 85.71% for 2.17% Gd and 87.21% for 3.93% Gd doped ZnS. The calculated rate constant (k) for 2.17% Gd and 3.93% Gd doped ZnS were 0.0053 min^{-1} and 0.0056 min^{-1} respectively (Table 3). From the Fig. 11c, complete degradation of methyl orange (MO) confirmed.

In the case of methylene blue dye, Gd doped ZnS has shown better photocatalytic activity than undoped ZnS, due to recombination effect and smaller crystallite size. Also, Gd doped ZnS revealed higher UV light absorption capability which counterfeits the recombination effect and helps the photocatalytic degradation of methylene blue dye. In the case of degradation of methyl orange and effluent the degradation efficiency of doped ZnS is less, because methyl orange and effluent absorbs more UV radiation than methylene blue. i.e. methylene blue dye allows more UV light to photocatalyst than all other dyes. The slight improvement in the photocatalytic activity of 3.93% Gd doped ZnS may be due the better crystalline nature of 3.93% Gd doped ZnS.

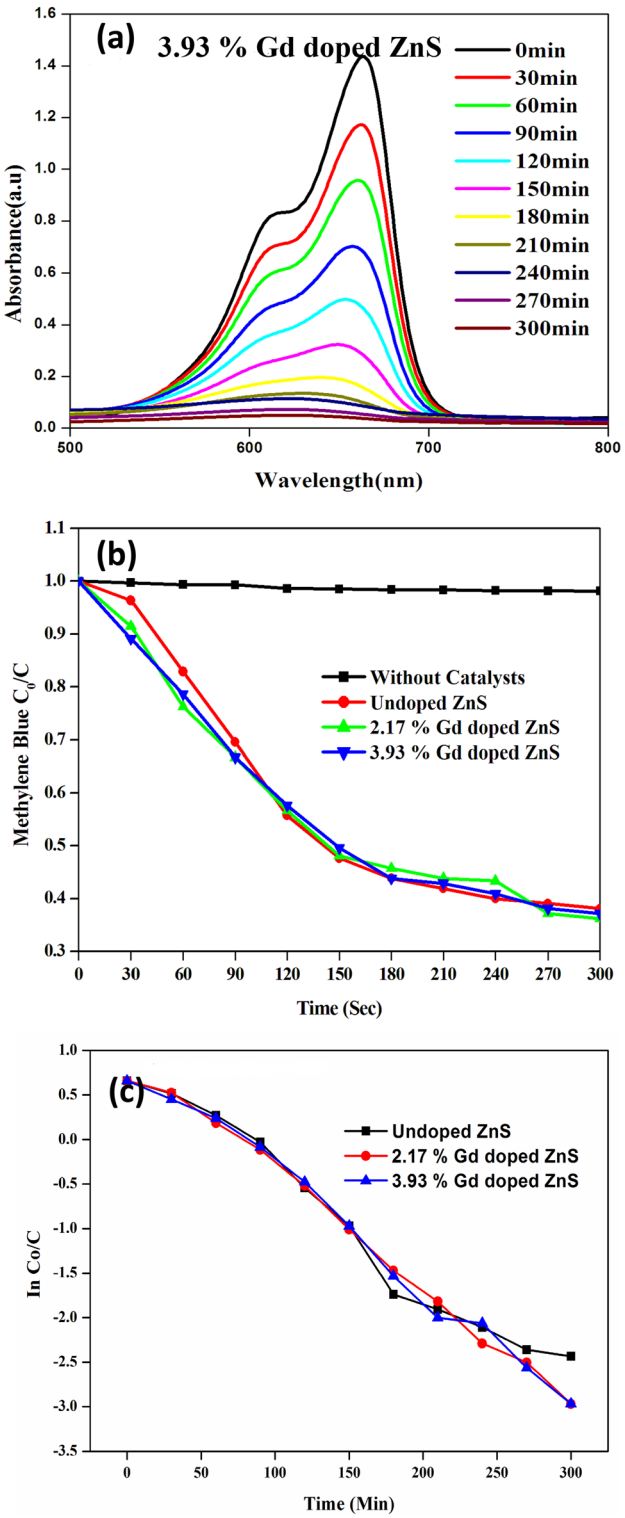

Fig. 9 **a** UV–visible absorbance spectra of methylene blue with Gd doped ZnS nanoparticles for 15 ppm, **b** photocatalytic degradation of methylene blue without and with Gd doped ZnS as a function of exposure time and **c** plot between ln (C_0/C) versus irradiation time to determine the value of rate constant k

Table 3 The reaction rate constant k (min^{-1}) of undoped and Gd doped ZnS samples for different dye solution

Samples	Methylene blue dye—(MB)			Methyl orange dye—(MO)			Industrial effluent dye		
	k (min^{-1})	R^2 (degree of fit)	Decolorization %	k (min^{-1})	R^2 (degree of fit)	Decolorization %	k (min^{-1})	R^2 (degree of fit)	Decolorization %
Pure ZnS	0.0111	0.9642	95.45%	0.0128	0.9700	99.70%	0.0063	0.8736	89.47%
2.17% Gd doped ZnS	0.0117	0.9833	97.34%	0.0122	0.9729	97.50%	0.0053	0.9286	85.71%
3.93%Gd doped ZnS	0.0117	0.9780	97.34%	0.0100	0.9927	89.70%	0.0056	0.9116	87.21%

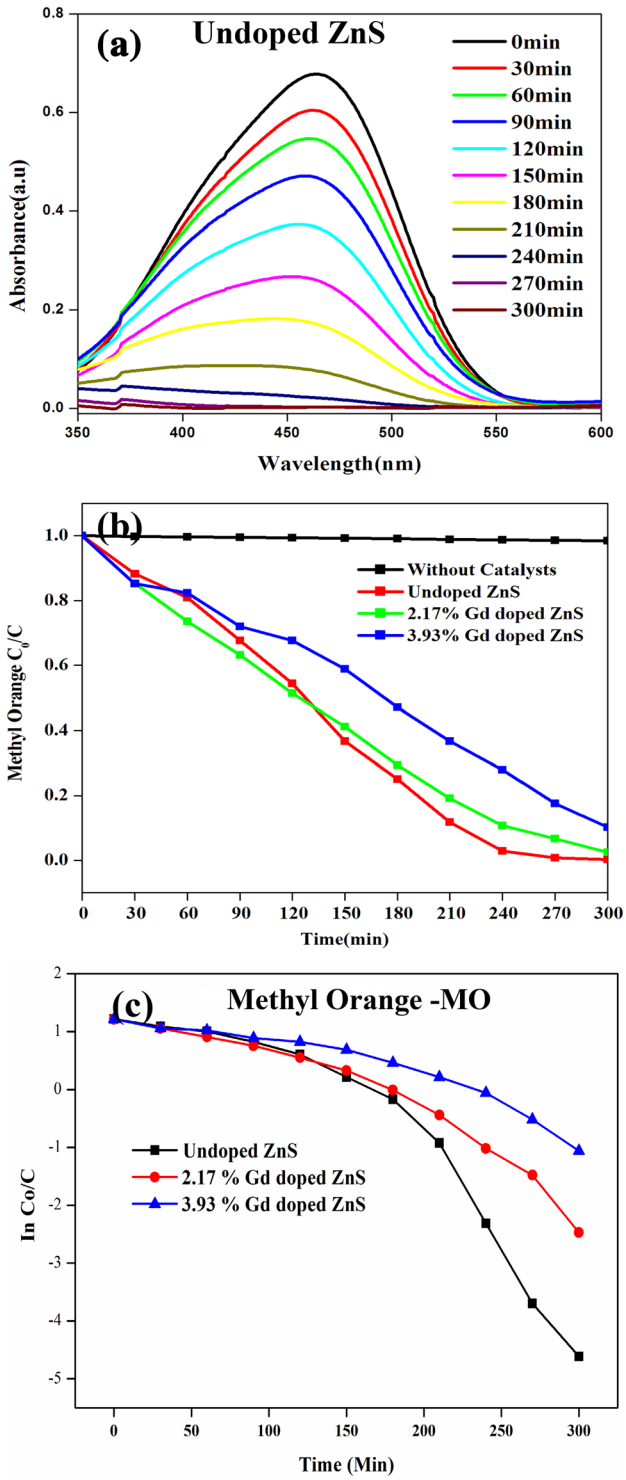

Fig. 10 **a** UV–visible absorbance spectra of methyl orange with undoped ZnS nanoparticles for 15 ppm, **b** photocatalytic degradation of methyl orange without and with Gd doped ZnS as a function of exposure time and **c** plot between ln (C_0/C) versus irradiation time to determine the value of rate constant k

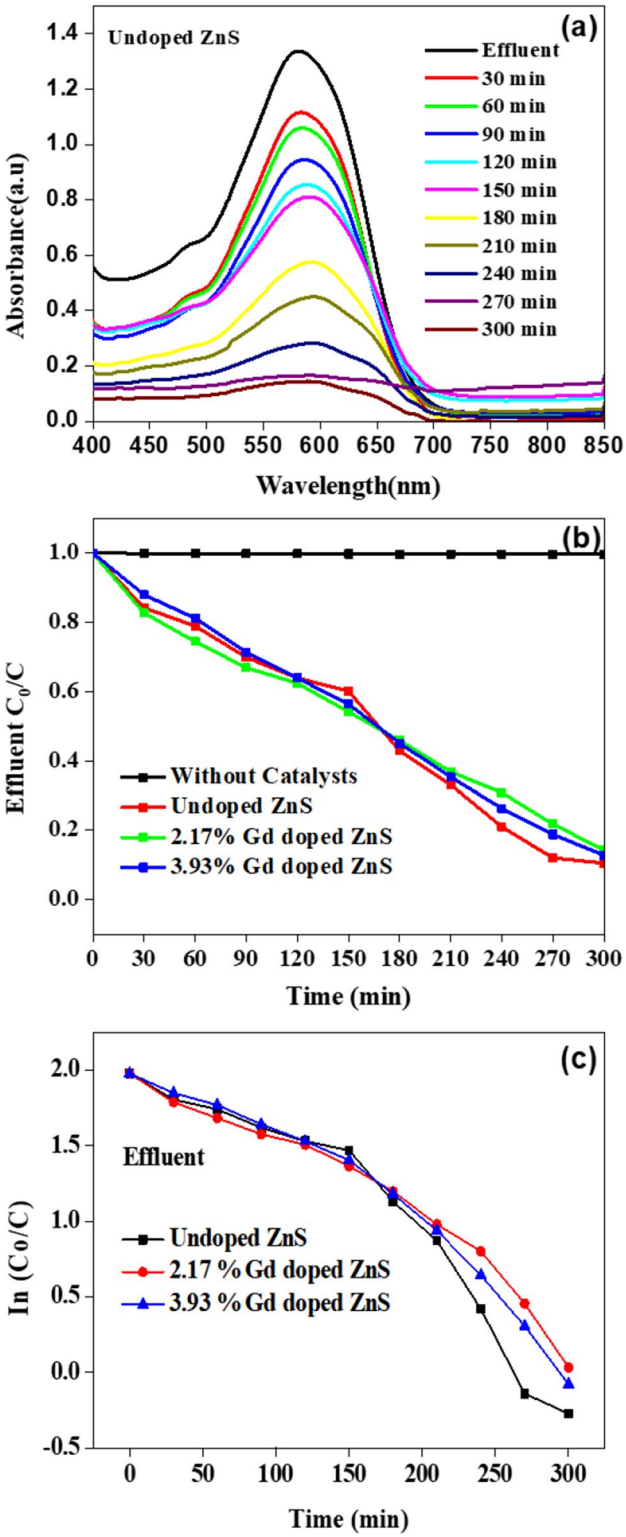

Fig. 11 **a** UV–Visible absorbance spectra of Effluent with undoped ZnS nanoparticles for 15 ppm, **b** photocatalytic degradation of Effluent without and with Gd doped ZnS as a function of exposure time and **c** plot between ln (C_0/C) versus irradiation time to determine the value of rate constant k

4 Conclusion

Undoped ZnS and Gd-doped ZnS nanoparticles were prepared at room temperature using chemical Co-precipitation method without using any catalysts, capping agents or surfactants. X-ray diffraction analysis revealed that the undoped and Gd doped ZnS nanoparticles are of hexagonal structure. The FESEM images of undoped and doped ZnS nanoparticles clearly show the formation of nanoclusters. Energy dispersive X-ray analysis showed the presence of Zn, S, and Gd in the respective samples. The optical absorption spectra of ZnS nanoparticles showed that the absorption edge is shifted to lower wavelength located at 294 nm compared to that of bulk ZnS, which has an absorption edge at 345 nm and it clearly indicates the formation of ZnS nanoparticles. The doping of Gd^{3+} ion in ZnS nanoparticles showed clear enhancement room temperature ferromagnetism which increased with increasing Gd content in the concentration. The photocatalytic activity of prepared samples was evaluated using synthetic dyes (methylene blue and methyl orange) and it was found that all the prepared samples are very good in the decolorization of the methylene blue, methyl orange dye and industrial effluent.

Acknowledgements R.S.K highly acknowledge Coimbatore Institute of Technology, Coimbatore for providing research facilities.

Compliance with ethical standards

Conflict of interest The authors declare that they have no conflict of interest.

References

1. Borker P, Salker AV (2006) Photocatalytic degradation of textile azo dye over Ce_{1-X} Sn_XO_2 series. Mater Sci Eng B 133:55–60
2. Coleman HM, Eggins BR, Anthony Byrne J, Palmer FL, King E (2000) Photocatalytic degradation of 17-B-oestradiol on immobilised TiO_2. Appl Catal B 24:L1–L5
3. Ohko Y, Ando I, Niwa C, Tatsuma T, Yamamura T, Nakashima T, Kubota Y, Fujishima A (2001) Degradation of bisphenol a in water by TiO_2 photocatalyst. Environ Sci Technol 35:2365–2368
4. Wang YB, Hong C-S (2000) TiO_2-mediated photo mineralization of 2-chlorobiphenyl: the role of O_2. Water Res 34:2791–2797
5. Hoffmann MR, Martin ST, Choi W, Bahnemann DW (1995) Environmental applications of semiconductor photocatalysis. Chem Rev 95:69–96
6. Robinson T, McMullan G, Marchant R, Nigam P (2001) Remediation of dyes in textile effluent: a critical review on current treatment technologies with a proposed alternative. Bio Resour Technol 77:247–255

7. Karakoti AS, Shukla R, Shanker R, Singh S (2015) Surface functionalization of quantum dots for biological applications. Adv Colloid Interface Sci 215:28–45
8. Tyrakowski CM, Snee PT (2014) A primer on the synthesis, water-solubilization, and functionalization of quantum dots, their use as biological sensing agents, and present status. Phys Chem Chem Phys 16:837–855
9. Aruldoss U, John Kennedy L, Judith Vijaya J, Sekaran G (2011) Photocatalytic degradation of phenolic syntan using TiO_2 impregnated activated carbon. J Colloid Interface Sci 355:204–209
10. Clament Sagaya Selvam N, Judith Vijaya J, John Kennedy L (2012) Effects of morphology and Zr doping on structural, optical, and photocatalytic properties of ZnO nanostructures. Ind Eng Chem Res 51:16333–16345
11. Clament Sagaya Selvam N, Manikandan A, John Kennedy L, Judith Vijaya J (2013) Comparative investigation of zirconium oxide (ZrO_2) nano and microstructures for structural, optical and photocatalytic properties. J Colloid Interface Sci 389:91–98
12. Clament Sagaya Selvam N, Narayanan S, John Kennedy L, Judith Vijaya J (2013) Pure and Mg-doped self-assembled ZnO nanoparticles for the enhanced photocatalytic degradation of 4-chlorophenol. J Environ Sci 25:2157–2167
13. Sherly ED, Judith Vijaya J, Clament Sagaya Selvam N, John Kennedy L (2014) Microwave assisted combustion synthesis of coupled ZnO–ZrO_2 nanoparticles and their role in the photocatalytic degradation of 2, 4-dichlorophenol. Ceram Int 40:5681–5691
14. Geng BY, Liu XW, Du QB, Wei XW, Zhang LD (2006) Structure and optical properties of periodically twinned ZnS nanowires. Appl Phys Lett 88:63104
15. Arul Dhas N, Zaban A, Gedanken A (1999) Surface synthesis of zinc sulfide nanoparticles on silica microspheres: sonochemical preparation, characterization, and optical properties. Chem Mater 11:806–813
16. Vilhunen S, Bosund M, Kääriäinen M-L, Cameron D, Sillanpää M (2009) Atomic layer deposited TiO_2 films in photodegradation of aqueous salicylic acid. Sep Purif Technol 66:130–134
17. Pirkanniemi K, Sillanpää M (2002) Heterogeneous water phase catalysis as an environmental application: a review. Chemosphere 48:1047–1060
18. Yin H, Wada Y, Kitamura T, Yanagida S (2001) Photoreductive dehalogenation of halogenated benzene derivatives using ZnS or CdS nanocrystallites as photocatalysts. Environ Sci Technol 35:227–231
19. Zhao Q, Xie Y, Zhang Z, Bai X (2007) Size-selective synthesis of zinc sulfide hierarchical structures and their photocatalytic activity. Cryst Growth Des 7:153–158
20. El-Kemary M, El-Shamy H (2009) Fluorescence modulation and photodegradation characteristics of safranin O dye in the presence of ZnS nanoparticles. J Photochem Photobiol A 205:151–155
21. Jang JS, Yu C-J, Choi SH, Ji SM, Kim ES, Lee JS (2008) Topotactic synthesis of mesoporous ZnS and ZnO nanoplates and their photocatalytic activity. J Catal 254:144–155
22. Chauhan R, Kumar A, Chaudhary RP (2013) Structural, optical and photocatalytic studies of Fe doped ZnS nanoparticles. J Sol-Gel Sci Technol 67:376–383
23. Muruganandham M, Amutha R, Repo E, Sillanpaa M, Kusumoto Y, Mamun MAA (2010) Controlled mesoporous self-assembly of ZnS microsphere for photocatalytic degradation of Methyl Orange dye. J Photochem Photobiol A 216:133–141
24. Divya A, Siva Kumar K, Sreedhara Reddy P (2011) Investigations on structural and optical properties of Zn1 – XGdXS nanoparticles. Appl Surf Sci 258:839–842
25. Poornaprakash B, Chalapathi U, Reddeppa M, Park S-H (2016) Effect on Gd doping on the structural, luminescence and magnetic properties of ZnS nanoparticles synthesized by the hydrothermal method. Superlattices Microstruct 97:104–109
26. Shi H, Zhang P, Li SS, Xia JB (2009) Magnetic coupling properties of rare-earth metals (Gd, Nd) doped ZnO: first-principles calculations. J Appl Phys 106:023910